THE JOURNAL OF BIOLOGICAL CHEMISTRY VOL. 288, NO. 30, pp. 21755–21769, July 26, 2013

A Link between Dimerization and Autophosphorylation of the Response Regulator PhoB*

Received for publication, March 22, 2013, and in revised form, June 10, 2013 Published, JBC Papers in Press, June 11, 2013, DOI 10.1074/jbc.M113.471763

Rachel L. Creager-Allen[‡], Ruth E. Silversmith[§], and Robert B. Bourret[§1]

From the Departments of [‡]Biochemistry and Biophysics and [§]Microbiology and Immunology, University of North Carolina, Chapel Hill, North Carolina 27599-7290

Background: Response regulator proteins within two-component signaling systems can autophosphorylate with small molecule phosphodonors.
Results: Autophosphorylation kinetics of the response regulator PhoB exhibit multiple features indicative of positive cooperativity between active sites.
Conclusion: PhoB autophosphorylation kinetics reflect formation of heterodimers (between phosphorylated and unphosphorylated monomers) with enhanced kinetics compared with monomers.
Significance: Response regulator dimers with a single phosphoryl group may contribute to transcription regulation.

Response regulator proteins within two-component signal transduction systems are activated by phosphorylation and can catalyze their own covalent phosphorylation using small molecule phosphodonors. To date, comprehensive kinetic characterization of response regulator autophosphorylation is limited to CheY, which follows a simple model of phosphodonor binding followed by phosphorylation. We characterized autophosphorylation of the response regulator PhoB, known to dimerize upon phosphorylation. In contrast to CheY, PhoB time traces exhibited an initial lag phase and gave apparent pseudo-first order rate constants that increased with protein concentration. Furthermore, plots of the apparent autophosphorylation rate constant *versus* phosphodonor concentration were sigmoidal, as were PhoB binding isotherms for the phosphoryl group analog BeF_3^-. Successful mathematical modeling of the kinetic data necessitated inclusion of the formation of a PhoB heterodimer (one phosphorylated and one unphosphorylated monomer) with an enhanced rate of phosphorylation. Specifically, dimerization constants for the PhoB heterodimer and homodimer (two phosphorylated monomers) were similar, but the rate constant for heterodimer phosphorylation was ~10-fold higher than for the monomer. In a test of the model, disruption of the known $PhoB_N$ dimerization interface by mutation led to markedly slower and noncooperative autophosphorylation kinetics. Furthermore, phosphotransfer from the sensor kinase PhoR was enhanced by dimer formation. Phosphorylation-mediated dimerization allows many response regulators to bind to tandem DNA-binding sites and regulate transcription. Our data challenge the notion that response regulator dimers primarily form between two phosphorylated monomers and raise the possibility that response regulator heterodimers containing one phosphoryl group may participate in gene regulation.

Two-component signal transduction systems, present in both eukaryotic and prokaryotic microorganisms as well as plants, are nearly ubiquitous in bacteria with tens of thousands of two-component system proteins currently annotated in sequence databanks (1, 2). The essential components of any two-component system are a sensor kinase and a partner response regulator. Detection of an environmental stimulus regulates the sensor kinase, often leading to autophosphorylation of a conserved histidine. The phosphoryl group is subsequently transferred to a conserved aspartate residue on the partner response regulator. Phosphorylation switches the response regulator to an active conformation (3), allowing the response regulator to exert its downstream effects. Many response regulators control transcription (4), typically by dimerization and binding to a symmetric DNA-binding site (5). To terminate the signal, response regulators dephosphorylate through autodephosphorylation (6), phosphatase-enhanced dephosphorylation (7, 8), or reverse phosphotransfer (9).

All response regulators contain a conserved receiver domain, and most also contain one or more variable output domains. The receiver domain (Fig. 1) has a conserved $(\beta\alpha)_5$ tertiary structure and contains the dimerization interface for many response regulators as well as the conserved active site that catalyzes both phosphorylation and dephosphorylation (5, 10). The five invariable residues that compose the active site include a conserved aspartate that is the site of phosphorylation, two acidic residues that coordinate a divalent cation required for catalysis, a threonine/serine, and a lysine. In addition to catalyzing phosphotransfer from the sensor kinase, response regulators can also catalyze their own autophosphorylation with small molecule phosphodonors, including phosphoramidate (H_3N^+–PO_3^{2-}, PAM),[2] acetyl phosphate, and monophosphoimidazole (11–15).

Although autophosphorylation has been qualitatively demonstrated for many response regulators, CheY is the only

* This work was supported, in whole or in part, by National Institutes of Health Grant R01GM050860 from NIGMS.
[1] To whom correspondence should be addressed: Dept. of Microbiology and Immunology, University of North Carolina, Chapel Hill, NC 27599-7290. Tel.: 919-966-2679; Fax: 919-962-8103; E-mail: bourret@med.unc.edu.

[2] The abbreviations used are: PAM, phosphoramidate; CheY-P, phosphorylated CheY; $PhoB_F$, full-length PhoB; $PhoB_N$, PhoB N-terminal receiver domain; PhoB-P, phosphorylated PhoB; nickel-NTA, nickel-nitrilotriacetic acid; RFI, relative fluorescence intensity.

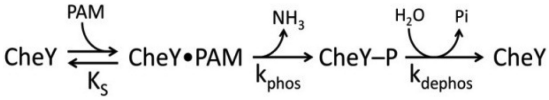

SCHEME 1. **Kinetic model of autophosphorylation of the response regulator CheY.**

response regulator for which extensively characterized autophosphorylation kinetics have been published (11, 13, 15, 16). The model of CheY autophosphorylation kinetics (in Scheme 1 with the phosphodonor PAM (12)) involves initial binding of phosphodonor to CheY to form a noncovalent complex (dissociation constant K_S), followed by phosphorylation (rate constant k_{phos}) and subsequent autodephosphorylation (rate constant k_{dephos}).

For CheY, the pre-steady state pseudo-first order rate constant for the accumulation of phosphorylated CheY (CheY-P) upon mixing CheY with phosphodonor remains linear with respect to PAM or acetyl phosphate concentration up to the highest concentrations of phosphodonor tested (100 mM), indicating very weak binding (K_S >500 mM) (11, 15, 16). Thus for CheY, it is only possible to measure the apparent bimolecular rate constant, k_{phos}/K_S, for accumulation of CheY-P, which is $\sim$10 M^{-1} s^{-1} for autophosphorylation with either acetyl phosphate or PAM (11, 13, 15, 16). However, CheY is not a typical response regulator in several respects. CheY consists only of a receiver domain and thus does not contain a variable output domain. Also, CheY does not act as a transcriptional regulator and does not dimerize upon phosphorylation.

To further explore response regulator autophosphorylation kinetics, we sought to characterize a more typical response regulator. PhoB is a member of the largest class of response regulators, termed the OmpR/PhoB family, which contains $\sim$30% of annotated response regulators (4). Like many response regulators, PhoB dimerizes through its receiver domain, allowing two output domains to come together and bind to a DNA-binding site on the promoter to regulate transcription (17). PhoB can autophosphorylate with acetyl phosphate or PAM (18–21) and contains an active site tryptophan (Fig. 1) that can be used as a fluorescent probe for both metal binding and autophosphorylation (20).

Analysis of structures of numerous receiver domains shows that phosphorylation or binding of a phosphoryl group analog to the active site Asp leads to conformational rearrangements on the α4-β5-α5 surface (3, 5, 22). These conformational shifts occur via a conserved mechanism of allosteric communication between the site of phosphorylation and the functionally relevant α4-β5-α5 surface. In dimerizing response regulators like PhoB (20, 23, 24), this conformational change allows two monomers to dimerize along the α4-β5-α5 surface (Fig. 1) (5). The coupling of phosphorylation and conformational change within the receiver domain occurs in both directions. Just as phosphorylation of response regulators promotes the active conformation, increasing the population of response regulator in the active conformation (*e.g.* binding target ligand) increases the rate of autophosphorylation (16, 25).

The PhoB receiver domain ($PhoB_N$) has been demonstrated to form two different types of dimers. The two $PhoB_N$ dimers have been extensively characterized both structurally and

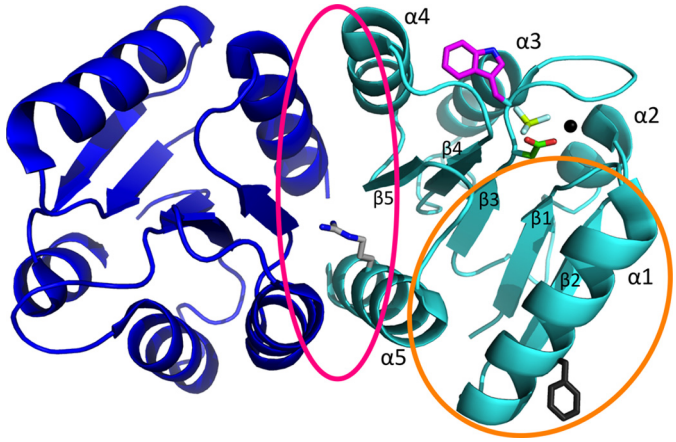

FIGURE 1. **Ribbon representation of the physiologically relevant $PhoB_N$ dimer (dimer 1).** The crystal structure shown is of $PhoB_N$ bound to the phosphoryl group analog BeF_3^- (Protein Data Bank code 1ZES). The two $(\beta\alpha)_5$ monomers that compose the dimer are colored *blue* (1ZES chain B) and *cyan* (1ZES chain C). Phosphoryl group analog BeF_3^- (*yellow* and *white*) is bound to Asp-53 (*green*). Also shown are the active site magnesium ion (*black sphere*) and the side chain for the Trp-54 fluorophore (*magenta*). The dimer 1 interface (*pink circle*) is composed of residues on helix α4, strand β5, and helix α5 and includes Arg-115 (*light gray*). The nonphysiological dimer 2 interface (*orange circle*) is composed of residues on helix α1, β5α5 loop, and helix α5 and includes Phe-20 (*dark gray*).

biochemically (26–29). As expected, a dimer along the α4-β5-α5 surface (here termed dimer 1) forms in the presence of a phosphoryl group analog (29) and represents the functional, phosphorylation-mediated dimer. Unexpectedly, metal binding alone supports a modified version of dimer 1 (27). Phosphorylated full-length PhoB ($PhoB_F$) dimer (dimer 1) has a dimerization constant of 5.1 μM (28) measured by analytical ultracentrifugation. A second $PhoB_N$ dimer, here termed dimer 2, forms along the α1-β5α5 loop-α5 surface (Fig. 1) and has been observed under crystallographic conditions in either the absence of metal and phosphorylation (26) or in the presence of just metal (single crystallographic conditions resulted in $PhoB_N$ monomers in both dimer 1 and dimer 2 within the asymmetric unit (27)). Dimer 2 may not be physiologically relevant due to a dimerization constant (>350 μM (28)) that is substantially higher than the *in vivo* concentration of PhoB (30).

Here, we present kinetic characterization of autophosphorylation of the *Escherichia coli* response regulator PhoB with the phosphodonor PAM. PhoB autophosphorylation exhibited several kinetic features that were fundamentally different from those of CheY. In contrast to the linear relationship between the pseudo-first order rate constant for accumulation of CheY-P and PAM concentration, this relationship for PhoB appeared sigmoidal and to approach saturation. Furthermore, unlike CheY, apparent pseudo-first order rate constants for PhoB autophosphorylation showed a protein concentration dependence. Additional biochemical evidence, supported by mathematical modeling, indicated a link between formation of PhoB dimer 1 and autophosphorylation kinetics. We propose that a heterodimer formed between a phosphorylated monomer and an unphosphorylated monomer of PhoB plays a role in PhoB autophosphorylation kinetics.

EXPERIMENTAL PROCEDURES

Cloning and Site-directed Mutagenesis—Genes encoding *E. coli* full-length PhoB ($PhoB_F$, residues 1–256) and the N-terminal receiver domain of PhoB ($PhoB_N$, residues 1–127) were amplified using standard PCR methods from the pENTR-b0399 (*phoB*) plasmid (31), provided by Dr. Michael Laub (Massachusetts Institute of Technology). The gene encoding *E. coli* CheY was amplified using standard PCR methods from pRS3 (32). PCR products were inserted into the pET28a vector (Novagen) to generate constructs ($PhoB_F$, pET28a·$phoB_F$; $PhoB_N$, pET28a·$phoB_N$; and CheY, pKC1) that encode proteins with a thrombin-cleavable His_6 tag at the N terminus. After thrombin cleavage, the resultant proteins contain an additional Gly-Ser-His at the N terminus. Addition of the three small residues is unlikely to affect the activity of the PhoB constructs because the N terminus is on the opposite side of the protein from the site of phosphorylation and is in a portion of PhoB that does not undergo a conformational change between the inactive and the active conformation. The presence of the same three residues in CheY did not affect the rates of autophosphorylation by PAM (data not shown) or autodephosphorylation (33). Site-directed mutagenesis was performed using QuikChange technology (Agilent Technologies). Wild type and mutagenized plasmids were transformed into *E. coli* strain BL21(DE3) for protein expression and purification.

The Gateway Entry vector for *phoR* (pENTR-b0400 (31)) encoding the soluble portion of *E. coli* PhoR (residues 193–431, throughout referred to as PhoR)) and the Gateway Destination vector (pML375) were provided by Dr. Michael Laub (Massachusetts Institute of Technology). The gene encoding PhoR was transferred from the entry vector into the destination vector using standard Gateway protocols (Invitrogen) to generate a construct (pDEST·phoR) that encodes a protein with a thrombin-cleavable His_6 tag at the N terminus.

Synthesis of Phosphoramidate—The potassium salt of PAM was synthesized as described (34).

Protein Overexpression and Purification—For the purification of CheY, $PhoB_F$, $PhoB_N$, $PhoB_N$ F20D, and PhoR, 1 liter of LB (+30 μg/ml kanamycin) was inoculated with 2.5 ml of an overnight culture of the appropriate expression strain and grown at 37 °C to an absorbance at 600 nm of 0.4. The culture was then transferred to room temperature, induced with 0.5 mM isopropyl 1-thio-β-D-galactopyranoside, and grown for 8–10 h. Cells were collected by centrifugation and resuspended in lysis buffer (50 mM Hepes, pH 7.0, 300 mM NaCl, 10 mM imidazole). The cells were lysed by sonication, and cellular debris was removed by ultracentrifugation (45 min, 4 °C, 37,000 × *g*). The supernatant was passed over a nickel-NTA-agarose (Qiagen) column, and the column was subsequently washed with wash buffer (50 mM Hepes, pH 7.0, 300 mM NaCl, 20 mM imidazole). Protein was eluted with elution buffer (50 mM Hepes, pH 7.0, 300 mM NaCl, 150 mM imidazole). All eluted proteins except PhoR were incubated with human α-thrombin (1 unit/ml sample, Hematologic Technologies, Inc.) overnight at 4 °C, followed by gel filtration over a Superdex 75 16/60 column in 50 mM Hepes, pH 7.0, 100 mM KCl, 2 mM DTT, 10% (v/v) glycerol to remove the thrombin and cleaved His_6 tag (for CheY, DTT was omitted from the gel filtration buffer). PhoR was further purified using a Superose 12 gel filtration column in 50 mM Tris, pH 7.5, 500 mM NaCl, and 10% (v/v) glucose. Aliquots of purified proteins were flash-frozen in dry ice/ethanol and stored at −80 °C.

$PhoB_N$ R115D was expressed and purified similarly to the above procedure with slight modifications based on a published purification protocol (28). One liter of LB (+30 μg/ml kanamycin) with 1 M sorbitol and 10 mM betaine was inoculated with 2.5 ml of an overnight culture in LB and grown at 37 °C to an absorbance at 600 nm of 0.4. The culture was transferred to room temperature, induced with 0.25 mM isopropyl 1-thio-β-D-galactopyranoside, and grown for 17–20 h. The cell pellet was resuspended in lysis buffer containing 140 μg of Halt protease inhibitor mixture (Thermo Scientific) followed by sonication, nickel-NTA chromatography, and thrombin cleavage as above. The Superdex 75 gel filtration buffer contained 50 mM Hepes, pH 7.0, 2 mM DTT, and 10% (v/v) glycerol.

Fluorescence Measurements—All fluorescence measurements were made using a PerkinElmer Life Sciences LS-50B fluorimeter equipped with a magnetic stirring device and FLWinLab software. Tryptophan fluorescence was measured at an excitation wavelength of 295 nm and an emission wavelength of 346 nm. Sample temperature was held at 25 ± 0.5 °C by a circulating water bath.

Equilibrium Fluorescence Measurements—Tryptophan fluorescence was used to monitor binding of divalent cation (Mn^{2+} or Mg^{2+}) or beryllium trifluoride (BeF_3^-) to various $PhoB_N$ constructs. All ligand binding assays were performed in triplicate in a 1 × 1-cm quartz cuvette at an initial volume of 1.5 ml.

Divalent cation binding was assayed similarly to a published protocol (35). $PhoB_N$ (5 μM) or $PhoB_N$ F20D (5 μM) in 100 mM Hepes, pH 7.0, was allowed to come to temperature equilibrium with constant magnetic stirring, and the initial fluorescence emission was measured. Then small volumes of a concentrated stock of $MnCl_2$ or $MgCl_2$ were incrementally added to the solution. After each addition, the solution was incubated for 2 min to ensure a homogeneous mixture. Ten fluorescence measurements were taken (1 measurement/s), and the values were averaged and corrected for dilution. Altogether, fluorescence was measured for 15 concentrations of divalent cation ranging between 5 and 1000 μM $MnCl_2$ and between 0.25 and 5 mM $MgCl_2$.

For BeF_3^- binding, $PhoB_N$ (5 μM) or $PhoB_N$ F20D (5 μM) was incubated in 100 mM Hepes, pH 7.0, 3 mM $MnCl_2$, and 10 mM NaF with constant stirring to reach temperature equilibrium. Small volumes of a concentrated stock of $BeCl_2$ were incrementally added to give concentrations between 1 and 100 μM. After each addition of $BeCl_2$, the solution was incubated for 2 min. $BeCl_2$ reacts with NaF to form a series of beryllium fluoride adducts, which should be dominated by BeF_3^- at 10 mM NaF (36). Thus, the concentration of BeF_3^- is assumed to be equal to the concentration of $BeCl_2$. Ten independent fluorescence measurements were taken (1 measurement/s) for each concentration of $BeCl_2$, and the values were averaged and corrected for dilution. To correct for nonspecific interactions between $PhoB_N$ and $BeCl_2$, titrations were also performed in the absence of NaF. There was a small increase in fluorescence upon the

first addition of $BeCl_2$, which was subtracted from the fluorescence intensity for the titrations that contained 10 mM NaF.

The above protocols were modified slightly for measurements of ligand binding to $PhoB_N$ R115D. $PhoB_N$ R115D exhibited a modest time-dependent quench in fluorescence, which stabilized within 15 min, in response to changes in solution ionic strength. The initial solutions containing 5 μM $PhoB_N$ R115D in buffer were thus allowed to incubate for 30 min at 25 °C. An additional control titration was carried out with KCl (0–15 mM) in lieu of Mn^{2+}, Mg^{2+}, or BeF_3^- to quantify the ionic strength response. For all titrations, solutions were incubated for 15 min after addition of ligand and before fluorescence measurements were taken. The changes in fluorescence due to changes in ionic strength as determined by KCl titration were subtracted from the fluorescence intensity at each concentration of ligand. For divalent metal and BeF_3^- binding, the changes in fluorescence due to changes in ionic strength were less than 5% of the total change in fluorescence.

For both divalent cation and BeF_3^- binding, plots of $(I_0 - I)$ *versus* ligand concentration were constructed, where I_0 is the fluorescence intensity with no added ligand, and I is the fluorescence intensity at a given concentration of ligand. Plots of BeF_3^- binding to $PhoB_N$ and $PhoB_N$ F20D were sigmoidal, and data were fit to Equation 1 (GraphPad Prism) to determine n, the Hill coefficient, and $K_{1/2}$, the concentration of $BeCl_2$ required to acquire half $(I_0 - I_{max})$.

$$(I_0 - I) = \frac{(I_0 - I_{max}) \times [\text{ligand}]^n}{K_{1/2}{}^n + [\text{ligand}]^n} \qquad \text{(Eq. 1)}$$

For determining all other ligand binding constants, a standard one-site binding equation was used.

Fluorescence Measurements of Reaction Kinetics—Tryptophan fluorescence was used to continuously monitor autophosphorylation of both CheY and various PhoB constructs with PAM. Observed rate constants for autophosphorylation of CheY at a given concentration of PAM decrease with increasing ionic strength of the solution (13). Thus, all reactions were performed at a constant ionic strength of 400 mM, which includes the concentration of buffer, divalent cation, PAM, and KCl.

Fluorescence measurement of CheY autophosphorylation was similar to previous reports (12, 15, 16). Briefly, a rapid mixing device (Applied Photophysics RX2000) was used to mix equal volumes of 10 μM CheY (in 6 mM $MnCl_2$ and 100 mM Hepes, pH 7.0) and PAM (20–300 mM in 100 mM Hepes, pH 7.0). Both CheY and PAM solutions were supplemented with KCl to give a final ionic strength of 400 mM. Because CheY and PAM solutions were mixed at a one-to-one (v/v) ratio, the concentrations of CheY, $MnCl_2$, and PAM were decreased by half in the final reaction. Fluorescence was continuously monitored, and time points were recorded every 20 ms. Reactions were performed in duplicate for each experimental condition.

Autophosphorylation reactions for $PhoB_F$, $PhoB_N$, and $PhoB_N$ F20D were carried out in a 1 × 0.4-cm quartz cuvette with manual mixing to initiate the reaction. The beginnings of the time traces were identical when measured using a stopped-flow apparatus or the standard cuvette. However, the ends of the time traces showed variability when measured using the stopped-flow apparatus, likely due to diffusion over the longer period of time required to achieve steady state for PhoB (up to 35 min). $PhoB_F$ (5 μM), $PhoB_N$ (2.5–20 μM), or $PhoB_N$ F20D (5 μM) was incubated in 100 mM Hepes, pH 7.0, 3 mM $MnCl_2$, and varying concentrations of KCl to reach a constant ionic strength of 400 mM (after PAM addition) with magnetic stirring to reach temperature equilibrium. The autophosphorylation reaction was initiated by addition of PAM (10–150 mM final concentration) to bring the final volume to 750 μl, followed by repetitive pipetting to mix (<5 s), and fluorescence was continuously monitored. Time points were recorded every 20 or 100 ms. Reactions were performed in triplicate for each experimental condition.

Autophosphorylation time traces of $PhoB_N$ R115D were measured in a 1 × 1-cm quartz cuvette at a final volume of 1.5 ml. $PhoB_N$ R115D (10 μM) was incubated in 6 mM $MnCl_2$, 100 mM Hepes, pH 7.0, and 282 mM KCl at a volume of 750 μl for 30 min with magnetic stirring. Because of the effect of ionic strength on $PhoB_N$ R115D fluorescence (see above), it was necessary to keep the ionic strength of the whole system at 400 mM throughout the experiment. For that reason, the autophosphorylation reaction was initiated by addition of an equal volume of PAM (20–300 mM) in 100 mM Hepes, pH 7.0, and varying concentrations of KCl to maintain a constant ionic strength of 400 mM, followed by mixing by repetitive pipeting (<5 s), and fluorescence was continuously monitored. Because $PhoB_N$ R115D and PAM solutions were mixed at a one-to-one (v/v) ratio, the concentrations of $PhoB_N$ R115D, $MnCl_2$, and PAM were decreased by half. Time points were recorded every 0.5 s. Reactions were performed in triplicate for each experimental condition.

Analysis of Kinetic Data—Autophosphorylation reactions were performed under pseudo-first order conditions, with a large molar excess of PAM over protein. Fluorescence time traces reflected a continually changing reaction rate, as the amount of unreacted CheY or PhoB decreased, although PAM concentration was essentially unchanged. All time traces were normalized by dividing the fluorescence intensities by the initial fluorescence intensity (I_0) to generate relative fluorescence intensity (RFI). Replicate time courses for the same protein or PAM concentration were averaged. The averaged, normalized fluorescence intensities are referred to as "time traces" for the rest of this study. Initial curve fits were made to a single exponential decay (GraphPad Prism). For CheY and $PhoB_N$ R115D, the time traces gave excellent fits to a single exponential, and the resulting pseudo-first order rate constants were termed observed rate constants (k_{obs}). For $PhoB_F$, $PhoB_N$, and $PhoB_N$ F20D, there were modest but systematic deviations from a single exponential decay. Therefore, we also tried fitting these data to a two-phase exponential decay, but the fits were indistinguishable from a single exponential. As described under "Results," there was utility in using the single exponential fits for initial data analysis, so the rate constants derived from imperfect single exponential fits were termed apparent rate constants (k_{app}). The simple kinetic model shown in Scheme 1 implicates the relationship between the pseudo-first order rate constant k_{obs} and individual kinetic parameters, shown in Equation 2 (12). For CheY·Mn^{2+}, plots of k_{obs} *versus* PAM concentration were linear, consistent with results obtained with

CheY·Mg^{2+} (11, 15, 16). This result indicates that the dissociation constant between CheY·Mn^{2+} and PAM is much larger than the highest concentration of PAM used in the experiment ($K_S \gg$ [PAM]), reducing Equation 2 to Equation 3. Thus the slope of the line is equal to the apparent bimolecular rate constant (k_{phos}/K_S). For $PhoB_N$ R115D, plots of k_{obs} *versus* the concentration of PAM were also linear, and the slope was similarly used to determine k_{phos}/K_S. Plots of the pseudo-first order rate constant k_{app} *versus* the concentration of PAM for $PhoB_F$, $PhoB_N$, and $PhoB_N$ F20D appeared sigmoidal and were thus fit using a modified Hill equation (Graph Pad Prism), Equation 4, where k_{max} is the maximum change in apparent rate constant; $K_{1/2}$ is the PAM concentration required to reach the mid-point of the dose-response curve; n is the Hill coefficient; and k_{min} is the minimum apparent rate constant.

$$k_{obs} = \frac{k_{phos} \times [PAM]}{K_S + [PAM]} + k_{dephos} \quad \text{(Eq. 2)}$$

$$k_{obs} = \frac{k_{phos}}{K_S} \times [PAM] + k_{dephos} \quad \text{(Eq. 3)}$$

$$k_{app} = \frac{k_{max} \times [PAM]^n}{K_{1/2}{}^n + [PAM]^n} + k_{min} \quad \text{(Eq. 4)}$$

Mathematical Modeling of $PhoB_N$ Autophosphorylation Time Traces—Mathematical modeling of $PhoB_N$ autophosphorylation time traces was performed using DynaFit software (37) to potentially explain several features of the kinetic data, including an apparent lag at the beginning of the $PhoB_N$ autophosphorylation time traces and the observation that protein concentration affected the apparent pseudo-first order rate constant for autophosphorylation. As described under "Results," numerous models of increasing complexity were tried before choosing the model described below. In particular, the protein concentration dependence of normalized $PhoB_N$ time traces constrained the model significantly because it necessitated the inclusion of a reaction step whereby multiple molecules of $PhoB_N$ interact to give reaction species with altered phosphorylation kinetics. Thus, based on a large body of evidence documenting the dimerization of $PhoB_F$ and $PhoB_N$ (20, 23, 24, 26–29), a comprehensive model of autophosphorylation kinetics of PhoB that included multiple versions of PhoB dimer 1 with the possibility of differing autophosphorylation kinetics was considered (Scheme 2). In the model, a monomer (m) of PhoB can bind to a molecule of PAM with dissociation constant K_S(m) and then phosphorylate with rate constant k_{phos}(m), analogous to the first two steps in Scheme 1 for CheY. A phosphorylated PhoB monomer can then interact with either another phosphorylated PhoB monomer to form a homodimer (PhoB-P/PhoB-P) or with an unphosphorylated PhoB monomer to form a heterodimer (PhoB/PhoB-P), with dimerization constants K_{dimer}(hom) and K_{dimer}(het), respectively. The heterodimer can then bind to a molecule of PAM with dissociation constant K_S(het) and phosphorylate with rate constant k_{phos}(het). All three phosphorylated species of PhoB can also dephosphorylate, with rate constants k_{dephos}(hom), k_{dephos}(het), and k_{dephos}(m). Dimerization of two unphosphorylated PhoB monomers (dimer 2) was excluded from the model due to a measured dimerization constant (378 μM (28)) that was much greater than the highest concentration of PhoB used in our experiments.

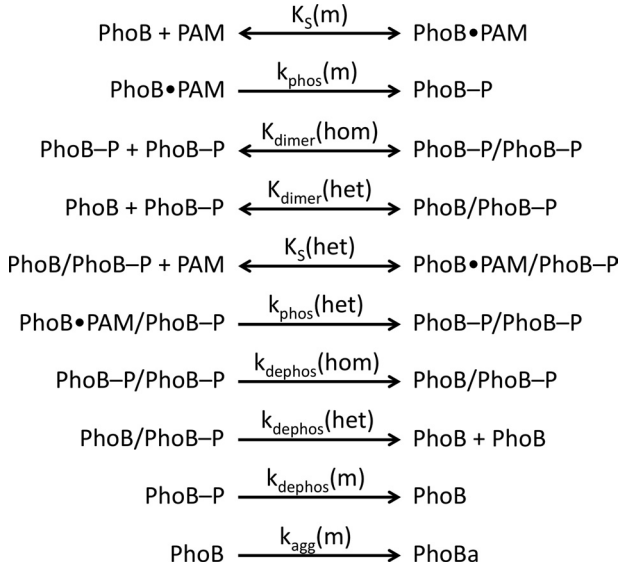

SCHEME 2. **Reactions included in mathematical model of autophosphorylation of PhoB.**

To fit the kinetic data to the model, the normalized fluorescence intensities for $PhoB_N$ autophosphorylation time traces were first multiplied by the protein concentration used in the experiment. DynaFit requires a conversion factor that translates the concentration of different PhoB species to the measured fluorescence responses. We established conversion factors based on the assumption that tryptophan fluorescence was quenched solely as a result of the conformational change that occurs upon PhoB phosphorylation or formation of the heterodimer but not by PAM binding. Thus, the species that are not primarily in the active conformation (PhoB and PhoB·PAM) were assigned a conversion factor equal to the initial fluorescence intensity divided by the protein concentration. The species that are primarily in the active conformation (PhoB-P, PhoB/PhoB-P, PhoB·PAM/PhoB-P, and PhoB-P/PhoB-P) were assigned a conversion factor equal to the minimum fluorescence intensity for autophosphorylation of 5 μM $PhoB_N$ with 150 mM PAM (*i.e.* the time trace with the maximum quench in fluorescence intensity) divided by the protein concentration. The described assumptions for the conversion factors gave good fits. Alternative assumptions were also tested (*e.g.* PAM binding to $PhoB_N$ resulted in quenched tryptophan fluorescence). However, alternative conversion factors could not by themselves account for fundamental features of the kinetics, such as the lag phase observed in the time traces or the protein concentration dependence of the apparent pseudo-first order rate constant.

An initial model composed of the nine reactions described above gave good fits for 10 of the 12 autophosphorylation time traces representing different concentrations of protein or PAM. However, there were systematic deviations for the two experimental conditions with the slowest time scales for autophosphorylation (10 and 20 mM PAM). Specifically, the rate and

equilibrium constants predicted by DynaFit gave modeled time traces that had the expected initial lag phases; however, the modeled plateaus at long reaction times were up to 30% below the experimental data. Slow formation of a PhoB aggregate (PhoBa) was added to the model with a rate constant of k_{agg}(m). To compensate for the higher plateau observed in the experimental time traces, the conversion factor for PhoBa was set to three times the initial fluorescence intensity divided by the protein concentration. This larger conversion factor is consistent with light scattering due to formation of a soluble aggregate.

Next, we set the following four parameters to experimentally measured values. K_{dimer}(hom) was set to the published value of 5.1 μM (28). (For all equilibrium constants, we assumed rapid equilibrium and set the k_{on} rate constant equal to 1×10^6 M^{-1} s^{-1} (38).) The three autodephosphorylation rate constants were determined by monitoring the disappearance of [^{32}P]PhoB$_N$-P or [^{32}P]PhoB$_N$ R115D-P over time (see "Experimental Procedures" below, data not shown). The rate constant k_{dephos}(hom) was set equal to the rate constant determined for [^{32}P]PhoB$_N$-P (0.0003 s^{-1}). Because PhoB$_N$ R115D cannot form dimer 1, k_{dephos}(m) was set equal to the rate constant determined for [^{32}P]PhoB$_N$ R115D-P (0.0002 s^{-1}). Because the model did not include formation of the unphosphorylated PhoB dimer, autodephosphorylation of the heterodimer was equivalent to dimer dissociation followed by monomer dephosphorylation. For that reason, k_{dephos}(het) was also set equal to the rate constant determined for [^{32}P]PhoB$_N$ R115D-P. Note that the measured k_{dephos} values for PhoB$_N$ are in close agreement with previously reported values for k_{dephos} for PhoB$_F$ (30, 35, 39).

The remaining six rate and equilibrium constants (K_S(m), k_{phos}(m), K_{dimer}(het), K_S(het), k_{phos}(het), and k_{agg}(m)) were then manually varied until the modeled time traces were similar to the raw time traces for autophosphorylation of 5 μM PhoB$_N$ with 60 mM PAM. These modeled values were then used as initial constants for global analysis of all of the time traces for PhoB$_N$ autophosphorylation (*i.e.* 2.5–20 μM PhoB$_N$ with 60 mM PAM and 5 μM PhoB$_N$ with 10–150 mM PAM). Nonlinear least square regressions were performed to simultaneously fit the six adjustable rate and equilibrium constants: K_S(m), k_{phos}(m), K_{dimer}(het), K_S(het), k_{phos}(het), and k_{agg}(m). Perturbing the initial values for the rate and equilibrium constants did not affect the resultant output. The residuals that were output by DynaFit were divided by protein concentration to allow for comparison between protein concentrations.

Radiolabeling of PhoR Using [γ-^{32}P]ATP—His$_6$-tagged PhoR (230 μg) was reacted with 1 mM [γ-^{32}P]ATP (18 Ci/mmol) in 35 mM Tris, pH 8.0, 35 mM KCl, and 3.5 mM $MgCl_2$ in a total volume of 200 μl for 30 min at room temperature. The sample was passed over 100 μl of prewashed nickel-NTA resin in a small centrifugal 0.22-μm filtration device and washed 10 times with 400 μl of wash buffer (50 mM Hepes, pH 7.0, 300 mM NaCl, 20 mM imidazole) to remove excess [γ-^{32}P]ATP. The [^{32}P]PhoR-P was eluted 3× with 400 μl of elution buffer (50 mM Hepes, pH 7.0, 300 mM NaCl, 150 mM imidazole) and concentrated. The concentration of [^{32}P]PhoR-P was determined using a Bradford assay with BSA standards. Purified aliquots of [^{32}P]PhoR-P were stored at −20 °C.

Phosphotransfer from [^{32}P]PhoR-P to PhoB$_N$—[^{32}P]PhoR-P was thawed and diluted into 35 mM Tris, pH 8.0, 35 mM KCl, and 3 mM $MnCl_2$ to give a final protein concentration of 1 μM and a final volume of 120 μl. A 7.5-μl aliquot was removed and added to 7.5 μl of 2× SDS-PAGE buffer for a zero time point. Either PhoB$_N$ or PhoB$_N$ R115D was added at a 10-fold molar excess (10 μM) and mixed, and a series of 7.5-μl time points up to 10 min were removed and immediately combined with 2× SDS-PAGE buffer. Samples were electrophoresed on 18% polyacrylamide gels, and the gels were subsequently dried. The amount of [^{32}P]PhoR-P at each time point was determined by phosphorimaging. The percentage of [^{32}P]PhoR-P remaining was plotted against time and then fit to a one-phase exponential decay to determine the rate constant for phosphotransfer.

Rate Constants for [^{32}P]PhoB-P Autodephosphorylation—His$_6$-tagged PhoR (6 μM) was reacted with 1 mM [γ-^{32}P]ATP (18 Ci/mmol) in 35 mM Tris, pH 8.0, 35 mM KCl, and 3 mM $MnCl_2$ in a total volume of 50 μl for 15 min at room temperature. The sample was passed over 100 μl of prewashed nickel-NTA resin in a small centrifugal 0.22-μm filtration device to bind His$_6$-tagged PhoR and washed 10 times with 400 μl of buffer containing 35 mM Tris, pH 8.0, 35 mM KCl, and 3 mM $MnCl_2$ to remove excess [γ-^{32}P]ATP. A 100-μl sample of either PhoB$_N$ (30 μM) or PhoB$_N$ R115D (30 μM) in 35 mM Tris, pH 8.0, 35 mM KCl, and 3 mM $MnCl_2$ was added to the column and incubated for 5 min at room temperature. The sample was allowed to filter over the nickel-NTA resin, and the nonbound material was collected. 7.5-μl samples were removed and added to an equal volume of 2× SDS-PAGE buffer at the following time points: 5, 10, 15, 30, 45, 60, 90, and 120 min. Samples were electrophoresed on 18% polyacrylamide gels. The gels were dried, and the amount of [^{32}P]PhoB$_N$-P at each time point was determined by phosphorimaging. The percentage of [^{32}P]PhoB$_N$-P remaining was plotted against time and then fit to a one-phase exponential decay to determine the rate constant for autodephosphorylation.

RESULTS

Optimization of PhoB Autophosphorylation Reaction Conditions—A divalent cation bound in the receiver domain active site is essential for catalysis of both response regulator phosphorylation and dephosphorylation (12, 40). Therefore, as a prerequisite for measuring PhoB autophosphorylation kinetics, it was necessary to characterize the metal binding properties of the various PhoB proteins (full-length PhoB (PhoB$_F$), the N-terminal receiver domain (PhoB$_N$), PhoB$_N$ F20D, and PhoB$_N$ R115D) so that the occupancy of the metal-binding site was known for subsequent autophosphorylation experiments. Tryptophan fluorescence measurements indicated that binding between Mg^{2+} and PhoB$_N$ occurred with a dissociation constant (K_D) of 1.6 ± 0.2 mM, in agreement with the reported K_D for PhoB$_F$ Mg^{2+} binding of 2.0 ± 0.5 mM (35). However, the concentration of Mg^{2+} required to reach high levels of metal-bound PhoB (> 95%) led to visible precipitation of both PhoB$_N$ and PhoB$_F$ within the time scale of the autophosphorylation reactions.

To avoid complications associated with precipitation, we searched for another metal ion that bound to PhoB and could support autophosphorylation. Although Mg^{2+} is most likely

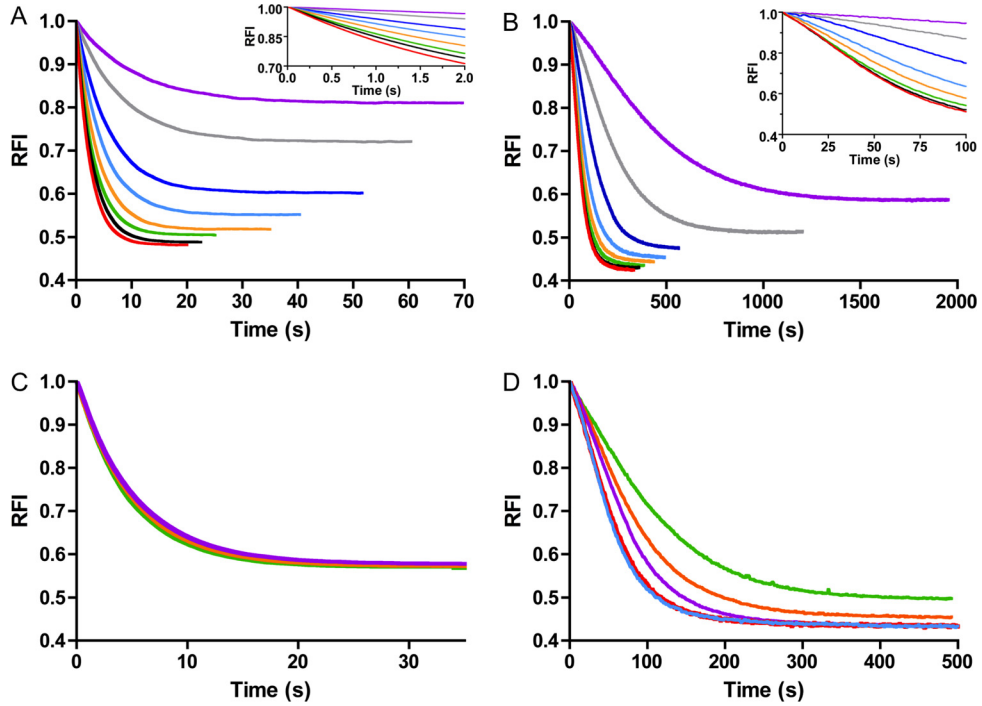

FIGURE 2. **Normalized CheY and $PhoB_N$ autophosphorylation time traces at various substrate or protein concentrations.** Fluorescence measurement of autophosphorylation of 5 μM CheY (*A*) and 5 μM $PhoB_N$ (*B*) at the following PAM concentrations: 10 mM (*purple*), 20 mM (*gray*), 40 mM (*dark blue*), 60 mM (*light blue*), 80 mM (*orange*), 100 mM (*green*), 125 mM (*black*), and 150 mM (*red*). *Insets* to *A* and *B* show a magnified view of the first portions of the autophosphorylation time traces. *C*, autophosphorylation of 2.5 μM (*green*), 5 μM (*orange*), and 10 μM (*purple*) CheY with 60 mM PAM. *D*, autophosphorylation of 2.5 μM (*green*), 5 μM (*orange*), 10 μM (*purple*), 15 μM (*red*), and 20 μM (*blue*) $PhoB_N$ with 60 mM PAM. *RFI* is the relative fluorescence intensity and represents the normalized tryptophan fluorescence intensity obtained by dividing all fluorescence intensities by the initial fluorescence intensity. Reactions were carried out in duplicate for *A* and *C* and in triplicate for *B* and *D*. Time traces represent the mean of multiple reactions, with standard deviations (not shown for clarity) that were less than 3% of the mean. Note that the time scales of all panels are different.

the divalent cation utilized by PhoB *in vivo*, Mg^{2+} and Mn^{2+} have similar size and preferred coordination number, geometry, and ligand type (41). Furthermore, Mn^{2+} supports autophosphorylation of the response regulator Spo0F with PAM (42), autophosphorylation of several sensor kinases, and phosphotransfer from a sensor kinase to a response regulator *in vitro* (43–45). Binding of Mn^{2+} to both $PhoB_F$ and $PhoB_N$ was much tighter than Mg^{2+}, with a K_D of 82 ± 6 and 70 ± 4 μM, respectively. Mn^{2+} bound to $PhoB_N$ F20D and $PhoB_N$ R115D with similar affinities (K_D of 51 ± 5 and 20 ± 8 μM, respectively). Furthermore, Mn^{2+} was highly capable of mediating $PhoB_N$ autophosphorylation, and the concentration of Mn^{2+} required for >95% occupancy of the metal-binding site (3 mM $MnCl_2$) did not lead to visible precipitation. Thus, the standard conditions for all autophosphorylation reactions in this study included 3 mM $MnCl_2$ to ensure high occupancy of the metal-binding site. Autophosphorylation of CheY was also readily catalyzed by 3 mM Mn^{2+} (see below); thus, all autophosphorylation experiments were done in parallel for PhoB and CheY to rule out the possibility that any novel characteristics of PhoB autophosphorylation were due to the use of Mn^{2+} as opposed to Mg^{2+}.

The visible precipitation that occurred between Mg^{2+} and PhoB was more severe for $PhoB_F$ than for $PhoB_N$. Although no visible precipitation occurred in solutions containing Mn^{2+} and either $PhoB_F$ or $PhoB_N$, we wanted to take every measure to minimize formation of aggregates during autophosphorylation experiments. For that reason, the majority of the autophosphorylation reactions was performed using the highly soluble $PhoB_N$. As expected from previous work (46), the removal of the DNA-binding domain did not affect autophosphorylation of PhoB (see below).

Normalized Autophosphorylation Time Traces for $PhoB_N$ Displayed a Visible Lag Phase and a Protein Concentration Dependence—Autophosphorylation of both $PhoB_N$ and CheY at various PAM and protein concentrations was monitored by continuous measurement of tryptophan fluorescence. In all cases, PAM concentration exceeded protein concentration by at least 3 orders of magnitude, so the reactions occurred under pseudo-first order conditions. For both CheY and $PhoB_N$, autophosphorylation was initiated by the addition of PAM, which resulted in a time-dependent quench in fluorescence that eventually leveled out (Fig. 2, *A–D*). The fluorescence intensity is a relative measure of the progress of the reaction from all unphosphorylated CheY or $PhoB_N$ (intensity at zero time) to a steady state level of phosphorylated CheY or $PhoB_N$ (intensity after steady state is achieved). Achievement of steady state indicates equal rates of autophosphorylation and autodephosphorylation. Because the absolute magnitude of the initial fluorescence intensity varied for individual reactions (especially for different protein concentrations), time traces (Fig. 2) were normalized by dividing by the initial fluorescence intensities and are reported as RFI.

As expected, the time traces for CheY·Mn^{2+} autophosphorylation (Fig. 2*A*) displayed similar properties as those reported for CheY·Mg^{2+} (11, 13). The shapes of the time

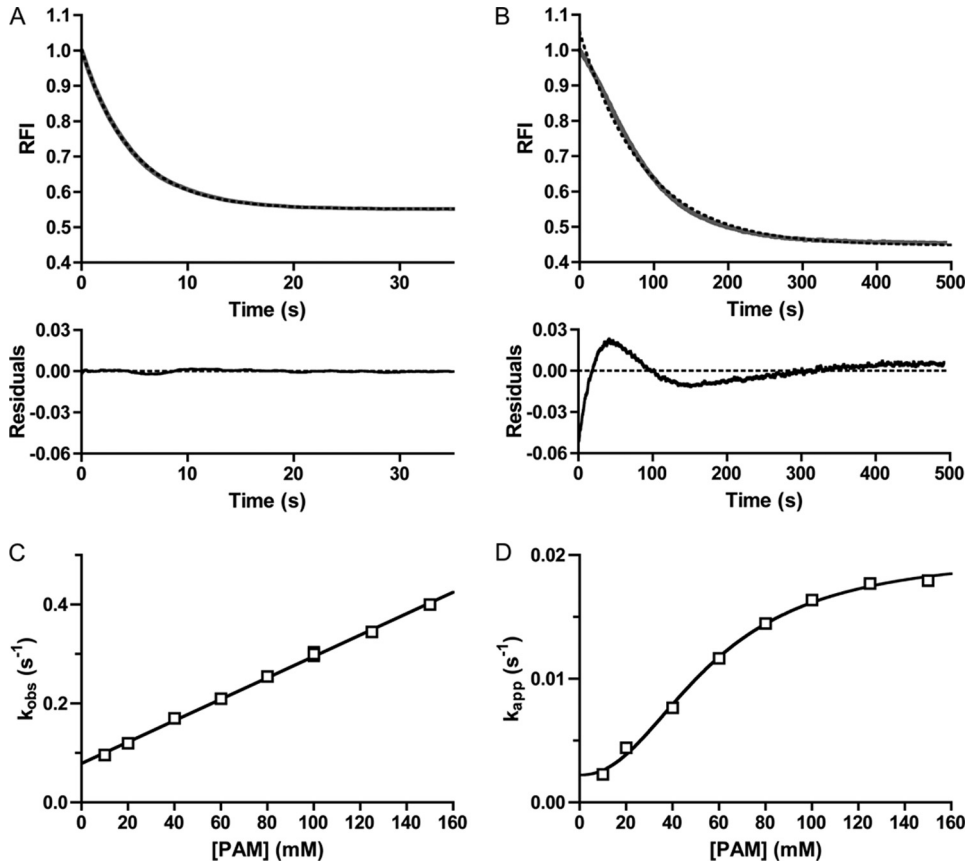

FIGURE 3. **Analysis of CheY and $PhoB_N$ time traces by fitting to a single exponential decay.** Autophosphorylation time traces for reaction of 5 μM CheY (*A*) or 5 μM $PhoB_N$ (*B*) with 60 mM PAM are shown in *gray*. The best fit to a one-phase exponential decay is shown in *dashed black lines*. The rate constant from the fit is k_{obs} for CheY and k_{app} for $PhoB_N$. Residuals (the difference between the raw data and the one-exponential decay) are shown at the bottom. *C,* plot of k_{obs} *versus* concentration of PAM for 5 μM CheY fit with linear regression (see Equation 3). The slope of the line gave k_{phos}/K_S, and the *y* intercept gave k_{dephos}. *Error bars* represent standard deviation from duplicate experiments. *D,* plot of k_{app} *versus* concentration of PAM for 5 μM $PhoB_N$ fit with sigmoidal dose-response curve (see Equation 4). *Error bars* represent standard deviation from triplicate experiments. Reactions were performed in duplicate for *A* and *C* and in triplicate for *B* and *D*. Time traces represent the mean of multiple reactions, with standard deviations (not shown for clarity) that were less than 3% of the mean. Most *error bars* in *C* and *D* were smaller than data points.

traces for CheY·Mn^{2+} autophosphorylation were the same as for CheY·Mg^{2+} and occurred on a similar time scale (20–100 s). Also, the maximum quench in fluorescence due to autophosphorylation was ~50% for both CheY·Mn^{2+} and CheY·Mg^{2+}. Because of the pseudo-first order reaction conditions employed ([PAM] ≫ [CheY]) and the fact that fluorescence is a measure of the relative progress of the reaction, increasing the concentration of PAM resulted in a shift of the time traces to shorter reaction times (Fig. 2*A*), but varying the concentration of CheY did not affect the time frame of the normalized time traces (Fig. 2*C*).

However, comparison of autophosphorylation time traces for CheY (Fig. 2*A*) and $PhoB_N$ (Fig. 2*B*) revealed three evident differences. First, autophosphorylation of $PhoB_N$ was markedly slower than autophosphorylation of CheY, although the $PhoB_N$ time traces were still dependent on PAM concentration. For example, at 60 mM PAM, it took ~500 s for autophosphorylation of $PhoB_N$ to reach steady state, while it only took ~35 s for CheY. Second, the $PhoB_N$ autophosphorylation time traces displayed a visible lag phase (Fig. 2*B, inset*) that was not present in time traces for CheY autophosphorylation (Fig. 2*A, inset*). This lag was most evident during the first 100 s of the autophosphorylation time traces for 40 and 60 mM PAM. Finally, the half-life of the normalized autophosphorylation time traces of $PhoB_N$ clearly decreased with increasing protein concentrations (2.5–20 μM) (Fig. 2*D*); however, CheY autophosphorylation time traces did not show a protein concentration dependence (Fig. 2*C*).

Both the lag and the protein concentration dependence of normalized time traces suggested that $PhoB_N$ autophosphorylation occurred with a more complex kinetic mechanism than CheY. Protein concentration dependence was inconsistent with a reaction in which a single molecule of $PhoB_N$ participates but was consistent with a reaction that involves interactions between two or more $PhoB_N$ molecules. The $PhoB_N$ protein concentration dependence, in particular, suggested that interactions between $PhoB_N$ monomers play a role in the kinetic mechanism of $PhoB_N$ autophosphorylation.

Initial Analysis of $PhoB_N$ Autophosphorylation Suggested Positive Cooperativity with Respect to PAM—To analyze the kinetics of autophosphorylation more quantitatively, we fit the autophosphorylation time traces to a one-phase exponential decay and plotted the resultant rate constants against PAM concentration. For CheY, the time traces fit extremely well to a one-phase exponential decay (Fig. 3*A*), with low residuals (difference between data and curve fitting) ($< \pm 0.25\%$) that dis-

played no obvious pattern. The CheY rate constants from these fits were termed k_{obs}. For CheY·Mn^{2+}, the plot of k_{obs} *versus* PAM concentration was linear, consistent with results obtained with CheY·Mg^{2+} (11, 15, 16), and the slope of the plot was equal to k_{phos}/K_S. The k_{phos}/K_S for reaction of CheY·Mn^{2+} with PAM was 2.2 ± 0.04 M^{-1} s^{-1}, which was ½ to ⅓ the k_{phos}/K_S of 6.1 M^{-1} s^{-1} for reaction of CheY·Mg^{2+} (after corrections for ionic strength (15)).

In contrast to CheY and consistent with the visible lag, the $PhoB_N$ autophosphorylation time traces exhibited systematic deviations from a one-phase exponential decay (Fig. 3*B*). The residuals for $PhoB_N$ followed a pattern and were 4–52 times larger than for CheY throughout the entire time course (Fig. 3, *A* and *B, lower panel*). Despite the systematic deviations from a single exponential decay, R^2 values for fitting $PhoB_N$ autophosphorylation time traces with a one-phase exponential decay were greater than 0.98. Rate constants obtained from the single exponential fits were used to estimate the overall rate of acquisition of steady state; however, due to the systematic deviations, we labeled these apparent rate constants k_{app} and used these values as an initial tool for analyzing the data.

A plot of k_{app} *versus* PAM concentration for $PhoB_N$ (Fig. 3*D*) differed from the plot of k_{obs} *versus* PAM concentration for CheY (Fig. 3*C*) in two ways. First, the plot of k_{app} *versus* PAM concentration for $PhoB_N$ fit to a sigmoidal dose-response curve with a Hill coefficient of 2.1 ± 0.2, which suggested that autophosphorylation of $PhoB_N$ exhibited some sort of positive cooperativity. The apparent positive cooperativity indicated communication between $PhoB_N$ active sites, such that autophosphorylation of one active site led to enhanced autophosphorylation kinetics at other sites, another suggestion that multimerization affects the rate of autophosphorylation of $PhoB_N$. Second, in contrast to k_{obs} for CheY, which showed no signs of saturating at the PAM concentrations used, k_{app} for $PhoB_N$ appeared to saturate at high PAM concentrations.

Previous work on PhoB autophosphorylation showed that removal of the DNA-binding domain did not affect the rate of PhoB autophosphorylation with 20 mM PAM (46). As expected, $PhoB_F$ autophosphorylation time traces with multiple PAM concentrations also showed a visible lag (Fig. 4*A*) and protein concentration dependence (data not shown) similar to $PhoB_N$. Also, plots of k_{app} *versus* PAM concentration for $PhoB_F$ (Fig. 4*B*) were nearly superimposable on $PhoB_N$ (Fig. 3*D*, Hill coefficient of 2.1 ± 0.3) and also appeared saturable. Thus, the kinetic properties exhibited by $PhoB_N$ were not due to removal of the DNA-binding domain.

Beryllium Trifluoride Binding to $PhoB_N$ Displayed Positive Cooperativity—The plot of k_{app} *versus* PAM concentration for $PhoB_N$ (Fig. 3) used rate constants derived from curve fits that systematically deviated from a single exponential decay. Thus, we sought an alternative method of assessing communication between $PhoB_N$ active sites by examining binding of a phosphoryl group analog. BeF_3^- binds to the active site of response regulators and mimics the Asp-phosphate linkage of phosphorylated response regulators (22, 29, 47). A plot of the quench in $PhoB_N$ tryptophan fluorescence *versus* BeF_3^- concentration (Fig. 5) was also sigmoidal with a Hill coefficient of 1.8 ± 0.2. The positive cooperativity exhibited in BeF_3^- binding lends

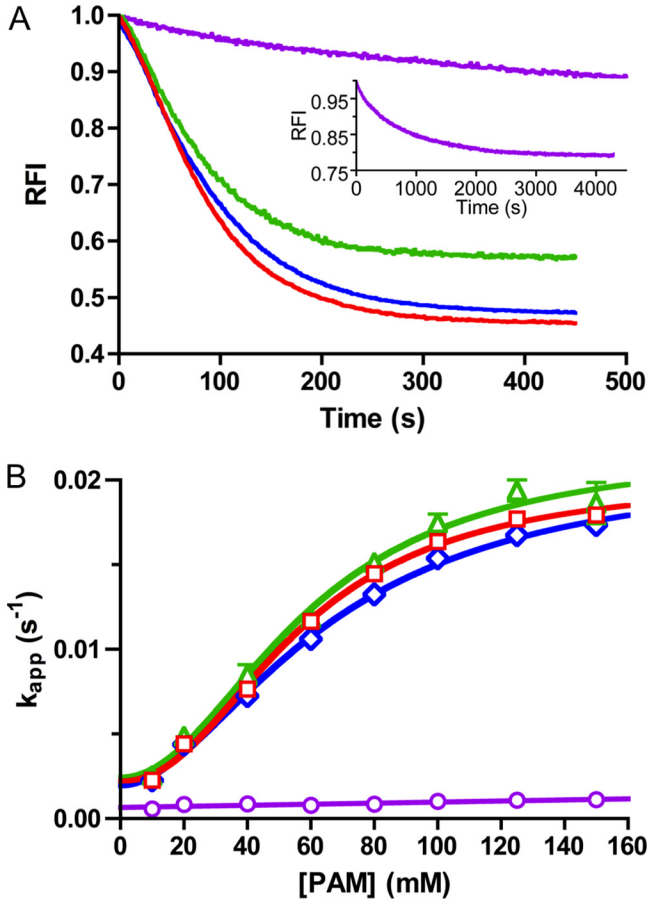

FIGURE 4. **Autophosphorylation kinetics of wild type PhoB ($PhoB_F$ and $PhoB_N$) and $PhoB_N$ dimer interface mutants.** *A*, autophosphorylation time traces for reaction of 5 μM $PhoB_F$ (*green*), 5 μM $PhoB_N$ F20D (*blue*), or 5 μM $PhoB_N$ R115D (*purple*) with 60 mM PAM. For comparison, the autophosphorylation time trace for reaction of 5 μM $PhoB_N$ with 60 mM PAM from Fig. 2*B* is shown in *red*. The *inset* is an expanded time scale to show the full autophosphorylation time trace for $PhoB_N$ R115D. $PhoB_F$ contains one extra tryptophan in the output domain that is not present in $PhoB_N$, leading to a smaller maximal quench in fluorescence for $PhoB_F$. Time traces represent the mean of three reactions, with standard deviations (not shown for clarity) that were less than 3% of the mean. *B*, plot of k_{app} *versus* concentration of PAM for 5 μM $PhoB_F$ (*green triangles*), 5 μM $PhoB_N$ F20D (*blue diamonds*), 5 μM $PhoB_N$ R115D (*purple circles*), or 5 μM $PhoB_N$ as shown in Fig. 3*D* for comparison (*red squares*) fit with sigmoidal dose-response curve (see Equation 4) for $PhoB_F$ and $PhoB_N$ F20D or linear regression (see Equation 3) for $PhoB_N$ R115D. *Error bars* represent standard deviation from triplicate experiments.

credibility to the apparent cooperativity of $PhoB_N$ autophosphorylation kinetics (Fig. 3*D*). Also, with a $K_{½}$ for BeF_3^- binding to $PhoB_N$ in the low micromolar range (44 ± 4 μM), the concentrations of BeF_3^- required to reach saturation were approximately 3 orders of magnitude lower than PAM concentrations needed, further reducing the possibility that a small amount of invisible aggregation could be affecting the $PhoB_N$ fluorescence signal.

Mathematical Modeling Supported a Link between Dimerization and Autophosphorylation of $PhoB_N$—In an attempt to account for the lag in the time traces and the protein concentration dependence of $PhoB_N$ autophosphorylation, we utilized mathematical modeling software to construct a model of autophosphorylation. We began with a model that was similar to the kinetic model of CheY autophosphorylation (Scheme 1) and included PAM binding, phosphorylation, and dephosphory-

lation of $PhoB_N$. This model was unable to account for either the lag of the autophosphorylation time traces or the protein concentration dependence, even when slow PAM binding or a variety of fluorescence intensity conversion factors were considered, suggesting a more complex kinetic mechanism of $PhoB_N$ autophosphorylation. The protein concentration dependence of $PhoB_N$ autophosphorylation, the visible lag in the $PhoB_N$ autophosphorylation time traces, the cooperative relationship between k_{app} and PAM concentration, and the sigmoidicity of BeF_3^- binding to $PhoB_N$ all suggested that there was a relationship between multimerization and autophosphorylation of $PhoB_N$. Specifically, the protein concentration dependence of autophosphorylation rate constants demanded that multiple $PhoB_N$ molecules participated in the autophosphorylation reaction, and the lag suggested the existence of a step early in the reactions that, once completed, resulted in faster autophosphorylation. PhoB is known to dimerize when phosphorylated, so we next included formation of a homodimer ($PhoB_N$-P/$PhoB_N$-P) in the model. This, too, was unable to account for the protein concentration dependence of autophosphorylation and the lag in the $PhoB_N$ autophosphorylation time traces, suggesting an even more complex mechanism.

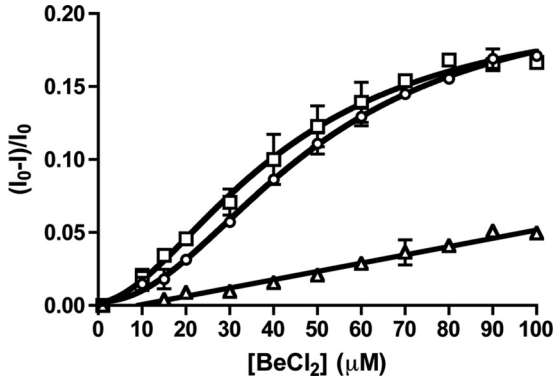

FIGURE 5. **Beryllium trifluoride binding to PhoB constructs.** Beryllium chloride titration with 5 μM $PhoB_N$ (*square*), 5 μM $PhoB_N$ F20D (*circle*), or 5 μM $PhoB_N$ R115D (*triangle*) was measured by fluorescence. The buffer contains 10 mM NaF. *Error bars* represent standard deviation from triplicate experiments.

To account for all aspects of the autophosphorylation data, formation of a $PhoB_N$ heterodimer ($PhoB_N$-P/$PhoB_N$) was fundamental to the model. The resultant 10-step kinetic model (Scheme 2, Fig. 6, and see "Experimental Procedures" for extensive details) included the formation of both the $PhoB_N$ homodimer ($PhoB_N$-P/$PhoB_N$-P) and the $PhoB_N$ heterodimer ($PhoB_N$-P/$PhoB_N$) and the possibility of differing autophosphorylation kinetics (K_S and k_{phos}) for the $PhoB_N$ monomer and the $PhoB_N$ heterodimer. Four out of the 10 kinetic parameters were set to constants obtained experimentally to limit the number of variables that were subject to change by DynaFit software.

All 12 time traces for autophosphorylation (*i.e.* 5 μM $PhoB_N$ with 10–150 mM PAM (Fig. 2*B*) and 2.5–20 μM $PhoB_N$ with 60 mM PAM (Fig. 2*D*)) were simultaneously fit to the model by global analysis using DynaFit software (Fig. 7). The global analysis of the $PhoB_N$ autophosphorylation time traces succeeded in fitting all data, and a single set of predicted kinetic constants (Fig. 6) gave simulated time traces that overlaid well with all 12 of the $PhoB_N$ autophosphorylation time traces. Formation of the PhoB aggregate was an extremely slow process with a rate constant (k_{agg}(m)) at least 2 orders of magnitude slower than either the rate constant for phosphorylation of the monomer (k_{phos}(m)) or the heterodimer (k_{phos}(het)). Furthermore, excluding aggregation from the model did not greatly affect 10 of the 12 autophosphorylation time traces. This was consistent with slow formation of a very small amount of soluble aggregate.

The rate and equilibrium constants generated by computer modeling were consistent with a link between $PhoB_N$ dimerization and autophosphorylation. Specifically, formation of a $PhoB_N$ heterodimer ($PhoB_N$-P/$PhoB_N$) and different autophosphorylation properties of the heterodimer compared with the monomer were fundamental to the model. Not only was inclusion of the heterodimer essential to fit the data, it was essential that the dimerization constant for the heterodimer (K_{dimer}(het)) had to be in the low micromolar range, similar to the dimerization constant for formation of the homodimer (K_{dimer}(hom), 5.1 μM (28)). In addition, k_{phos}(het) had to be at

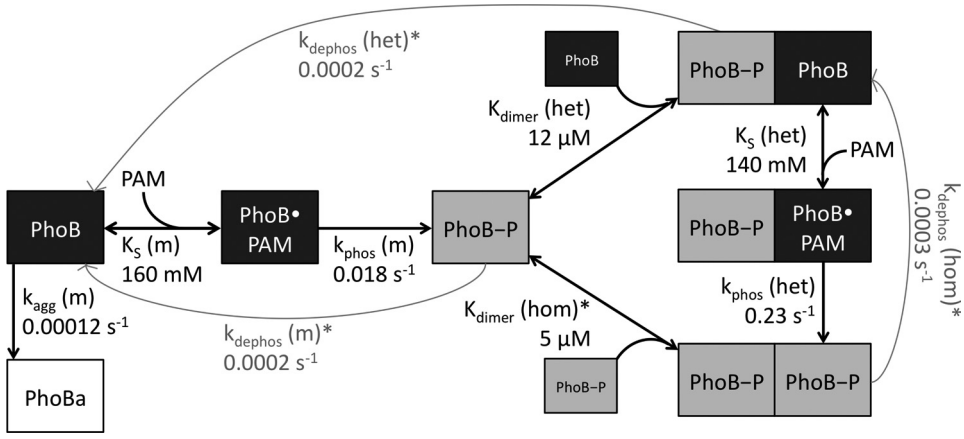

FIGURE 6. **Model linking $PhoB_N$ heterodimer formation and autophosphorylation.** A monomer of $PhoB_N$ binds a small molecule phosphodonor (*PhoB·PAM*) and phosphorylates (*PhoB-P*). The phosphorylated monomer can bind another phosphorylated monomer to form a homodimer. The phosphorylated monomer can also bind an unphosphorylated monomer to form a heterodimer, which can then bind PAM and phosphorylate. All three phosphorylated species of $PhoB_N$ can autodephosphorylate. Rate and equilibrium constants predicted by mathematical modeling are included by corresponding *arrows*. Kinetic constants marked with an *asterisk* were measured experimentally.

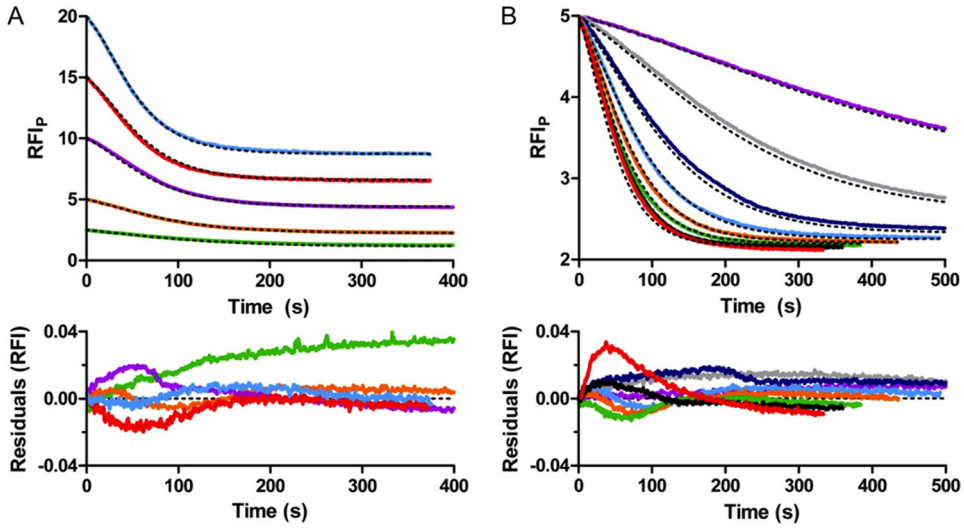

FIGURE 7. **Mathematical modeling by global kinetic analysis of autophosphorylation of PhoB$_N$.** Autophosphorylation time traces for reaction of 2.5–20 μM PhoB$_N$ with 60 mM PAM (*A*) and for reaction of 5 μM PhoB$_N$ with 10–150 mM PAM truncated to 500 s (*B*) with overlays of modeled fits from global kinetic analysis by DynaFit (*black dashed lines*) and residuals. Colors in *A* are described in Fig. 2*D*. Colors in *B* are described in Fig. 2*B*. *RFI$_P$* represents the normalized tryptophan fluorescence intensity obtained by dividing all fluorescence intensities by the initial fluorescence intensity then multiplying by the protein concentration.

least 10-fold faster than k_{phos}(m). Dimerization constants in the same range as the protein concentration used in the experiments account for the protein concentration dependence of k_{app}. The difference between k_{phos}(m) and k_{phos}(het) accounts for the lag in the autophosphorylation time traces. Even modest modifications (±50%) to the rate and equilibrium constants predicted by DynaFit led to poor fits to the autophosphorylation data.

Disruption of the Physiologically Relevant Dimer 1 Interface of PhoB$_N$ Impeded Autophosphorylation—Crystallographic evidence shows that PhoB$_N$ is able to dimerize at two different dimerization interfaces (26, 27, 29), the α4-β5-α5 surface (dimer 1) and the α1-β5α5 loop-α5 surface (dimer 2) (Fig. 1). To more directly test the potential link between dimer formation and autophosphorylation of PhoB$_N$, we characterized autophosphorylation kinetics of PhoB$_N$ variants containing previously characterized amino acid substitutions known to disrupt dimer formation (28). Replacement of Arg-115 with Asp (PhoB$_N$ R115D) disrupted the electrostatic interaction between residues Arg-115 and Asp-101 in the dimer 1 interface. Replacement of Phe-20 with Asp (PhoB$_N$ F20D) disrupted the hydrophobic dimerization interface of dimer 2.

Autophosphorylation of PhoB$_N$ F20D (dimer 2 mutant) with varying PAM concentrations displayed kinetics similar to wild type PhoB$_N$. The autophosphorylation time traces exhibited a visible lag at the beginning of the time traces similar to wild type PhoB$_N$ (Fig. 4*A*). A plot of k_{app} *versus* PAM concentration for PhoB$_N$ F20D also fit to a sigmoidal curve with a Hill coefficient of 1.8 ± 0.2 (Fig. 4*B*), implying positive cooperativity of autophosphorylation similar to wild type PhoB$_N$. Therefore, the cooperativity of autophosphorylation of wild type PhoB$_N$ was not likely due to formation of a dimer along the nonphysiological dimer 2 interface.

In contrast, autophosphorylation of PhoB$_N$ R115D (dimer 1 mutant) with PAM occurred over a much longer time scale than wild type PhoB$_N$ and did not exhibit a visible lag at the beginning of the time traces (Fig. 4*A*, *inset*). The plot of k_{obs} *versus* PAM concentration for PhoB$_N$ R115D (Fig. 4*B*) showed no signs of sigmoidicity and fit to a linear regression. Thus, disruption of the physiologically relevant PhoB$_N$ dimer 1 interface resulted in slow autophosphorylation kinetics that were not cooperative. This result supported the link between dimerization and autophosphorylation of PhoB$_N$ and, furthermore, identified the dimer 1 interface as the functionally relevant dimerization surface in autophosphorylation. Putting the mutant results together with previous observations and modeling, we propose that autophosphorylation kinetics of wild type PhoB$_N$ reflect the formation of a heterodimer along the dimer 1 interface, which leads to an enhanced rate constant for phosphorylation of the PhoB$_N$ heterodimer compared with the PhoB$_N$ monomer.

Beryllium Trifluoride Binding to the Physiologically Relevant Dimer 1 Mutant PhoB$_N$ R115D Was Not Cooperative—To further investigate the role of dimer formation on the cooperativity of wild type PhoB$_N$ kinetics, we characterized the BeF_3^- binding properties of PhoB$_N$ R115D and PhoB$_N$ F20D. Binding of BeF_3^- to PhoB$_N$ F20D was cooperative with a Hill coefficient (2.0 ± 0.1) and binding constant (51 ± 3 μM) similar to wild type PhoB$_N$ (Fig. 5). In contrast, binding of BeF_3^- to PhoB$_N$ R115D was not cooperative and displayed a much weaker binding constant than wild type PhoB$_N$ (Fig. 5). Because disruption of dimer 1 eliminated the cooperativity of BeF_3^- binding to PhoB$_N$, the cooperativity of BeF_3^- binding to wild type PhoB$_N$ was likely due to the formation of a dimer along the dimer 1 interface.

Phosphotransfer from [^{32}P]PhoR-P to Wild Type PhoB$_N$ Was Faster Than to PhoB$_N$ R115D—To determine whether there was a link between the formation of the PhoB$_N$ dimer and phosphotransfer from the histidine kinase PhoR, the rate constants for phosphotransfer from [^{32}P]PhoR-P to wild type PhoB$_N$ and PhoB$_N$ R115D were determined by monitoring the time-dependent disappearance of [^{32}P]PhoR-P in the presence of a

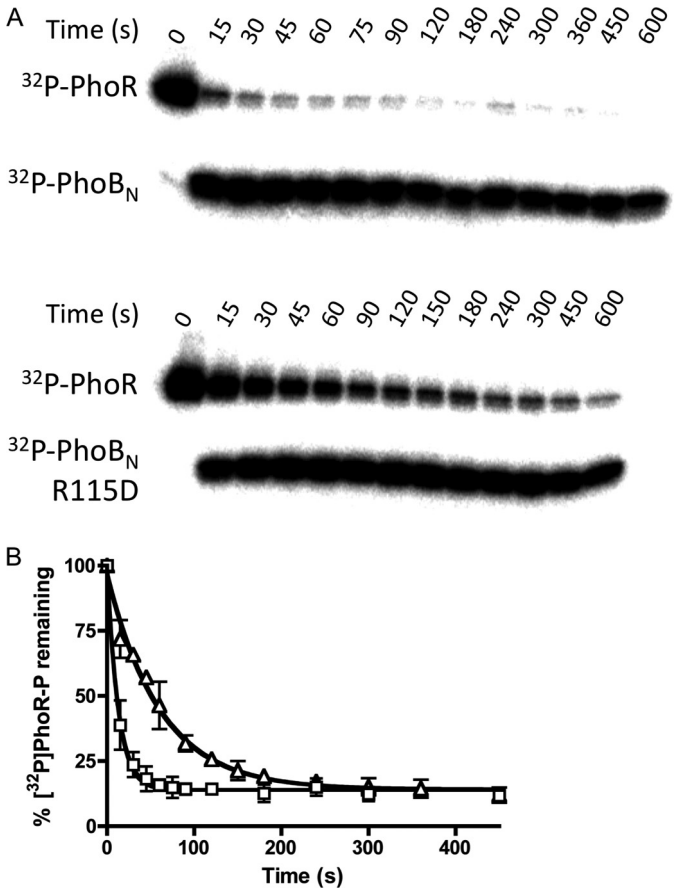

FIGURE 8. **Phosphotransfer from [^{32}P]PhoR-P to either wild type $PhoB_N$ or $PhoB_N$ R115D.** *A,* phosphorimage of SDS-polyacrylamide gel analysis of phosphotransfer reactions. Each lane represents a different time point between 0 and 600 s as shown. *B,* quantitative analysis of the phosphorimage as shown in *A* for wild type $PhoB_N$ (*squares*) and $PhoB_N$ R115D (*triangles*), fit to a one-phase exponential decay. Each point represents the average and standard deviation of replicate experiments.

10-fold molar excess $PhoB_N$ (Fig. 8). Phosphotransfer from [^{32}P]PhoR-P to wild type $PhoB_N$ was approximately five times faster than phosphotransfer from [^{32}P]PhoR-P to $PhoB_N$ R115D, with bimolecular rate constants of 77,000 ± 5000 and 16,000 ± 1,000 M^{-1} s^{-1}, respectively. Therefore, both $PhoB_N$ autophosphorylation with PAM and phosphotransfer from [^{32}P]PhoR-P to $PhoB_N$ were enhanced by the formation of dimer 1. Furthermore, accumulation of the radiolabeled phosphoryl group on $PhoB_N$ R115D occurred in a time-dependent manner to a similar extent as wild type $PhoB_N$ (Fig. 8) indicating functional $PhoB_N$ R115D protein.

DISCUSSION

A central observation here was that in contrast to CheY, $PhoB_N$ and $PhoB_F$ autophosphorylation kinetics exhibited properties indicative of communication between active sites from different monomers. Numerous lines of evidence supported the notion that association of PhoB monomers to form heterodimers (one phosphorylated and one unphosphorylated monomer) affected autophosphorylation kinetics, including the protein concentration dependence of the normalized autophosphorylation time traces (Fig. 2*D*), the systematic deviation of the autophosphorylation time traces from a one-phase exponential (Fig. 2*B*), and the sigmoidicity of the plot of k_{app} *versus* PAM concentration (Fig. 3*D*). Binding of the phosphoryl group analog BeF_3^- to $PhoB_N$ was sigmoidally dependent on BeF_3^- concentration (Fig. 5) also indicating communication between $PhoB_N$ active sites. As predicted by a reaction scheme in which heterodimers play a role in autophosphorylation kinetics, disruption of the dimer 1 dimerization interface by the previously characterized R115D amino acid substitution (28) greatly reduced the rate of $PhoB_N$ autophosphorylation (Fig. 4*B*) and eliminated cooperativity in both autophosphorylation and BeF_3^- binding (Fig. 5).

Successful Mathematical Modeling of Autophosphorylation Data Provided Insights into the PhoB Reaction Mechanism—After testing multiple models of increasing complexity, we developed a scheme that linked autophosphorylation and dimerization of $PhoB_N$ (Fig. 6). A mathematical model based on this scheme and utilizing a single set of kinetic and equilibrium constants (some experimentally determined, some computationally inferred) was able to faithfully reproduce all the experimentally observed effects of changing either $PhoB_N$ or PAM concentration (Fig. 7).

First, the difference between k_{phos}(m) and k_{phos}(het) accounted for the lag in the autophosphorylation time traces and deviation from a single phase exponential. Specifically, PhoB autophosphorylation kinetics were initially dominated by monomers (k_{phos}(m)) and hence were slow. After creation of phosphorylated monomers facilitated heterodimer formation with an excess of unphosphorylated PhoB monomers, faster autophosphorylation kinetics (k_{phos}(het)) became evident. The model predicted that under the experimental conditions employed, there was a flux from monomers through heterodimers to homodimers but not necessarily a large accumulation of heterodimers. Second, a predicted dimerization constant (K_{dimer}(het)) for heterodimer formation in the same range as the protein concentration used in the experiments accounted for the protein concentration dependence of the normalized $PhoB_N$ time traces observed in Fig. 2*D*. Changing $PhoB_N$ concentration around K_{dimer}(het) altered heterodimer formation and hence the experimentally measured rate constants for the reaction. Additional insights gleaned from the mathematical model into the detailed mechanism of PhoB positive cooperativity are described below.

Dimerization Constant for the $PhoB_N$-P/$PhoB_N$ Heterodimer Was in the Low Micromolar Range—A surprising prediction from the kinetic modeling was that the dimerization constant for formation of the $PhoB_N$-P/$PhoB_N$ heterodimer (K_{dimer}(het), 12 μM) was similar to that measured for formation of the $PhoB_N$-P/$PhoB_N$-P homodimer (K_{dimer}(hom), 5.1 μM (28)). Receiver domain phosphorylation results in a conserved allosteric activating conformational change that includes changes in the $\alpha4$-$\beta5$-$\alpha5$ surface (3, 5). For multiple response regulators in the OmpR/PhoB family, the changes in the $\alpha4$-$\beta5$-$\alpha5$ surface result in formation of a dimer (3, 5, 20, 23, 24). Thus, it might be expected that acquisition of the active conformation is a prerequisite for dimerization and that formation of a PhoB heterodimer would involve association of a phosphorylated PhoB monomer with an unphosphorylated monomer that is in the active conformation. In such a circumstance, K_{dimer}(het) would

be a composite of both the equilibrium constants for the conformational change and for dimerization (linked equilibria (48)), described by $K_{dimer,\,link}$ in Equation 5, where $K_{dimer,\,link}$ is the apparent dimerization constant for heterodimer formation; K_{conf} is the conformational equilibrium constant for PhoB in the active conformation, and $K_{dimer,\,act}$ is the associative dimerization constant of PhoB in the active conformation,

$$K_{dimer,link} = K_{conf} \cdot K_{dimer,act} \quad \text{(Eq. 5)}$$

Although it is difficult to measure the fraction of the response regulator population in the active conformation, it is estimated that no more than 10% of unphosphorylated response regulator molecules are in the active conformation (16, 49). Therefore, if K_{conf} is less than 0.1, we would predict K_{dimer}(het) to be at least 10-fold larger than K_{dimer}(hom), which does not contain a significant conformational component because the phosphorylated monomers are predominantly in the active conformation. The similarity between the predicted K_{dimer}(het) and the measured K_{dimer}(hom) suggests that acquisition of the active conformation is not a prerequisite for PhoB heterodimer formation. Although there is no direct evidence for the formation of a $PhoB_N$ heterodimer, a modified version of dimer 1 has been crystallized in the absence of BeF_3^- (27). Both monomers in the structure were in the inactive conformation, implying that $PhoB_N$ dimer 1 formation does not require acquisition of the active conformation before association.

Accelerated Autophosphorylation of the $PhoB_N$-P/$PhoB_N$ Heterodimer—The second important prediction from the mathematical modeling of $PhoB_N$ autophosphorylation was that the rate constant for phosphorylation of the heterodimer (k_{phos}(het)) was approximately 10 times higher than the rate constant for phosphorylation of the monomer (k_{phos}(m)), implying that formation of the heterodimer of $PhoB_N$ enhanced the rate of autophosphorylation. This result is consistent with other observations that have linked an activated conformation to faster autophosphorylation kinetics. Addition of FliM (a ligand that pushes CheY toward an active-like conformation (50)) to CheY greatly enhances the rate of autophosphorylation compared with no ligand present (16). Similarly, addition of DNA that binds to OmpR increases the rate of autophosphorylation compared with no ligand present (25). We propose that formation of the heterodimer of $PhoB_N$ pushes the conformational equilibrium of the unphosphorylated monomer in the heterodimer toward the active conformation, which results in a faster rate of autophosphorylation of the $PhoB_N$ heterodimer compared with the $PhoB_N$ monomer.

Physiological Implications of Cooperative Kinetics—We have presented extensive yet indirect evidence for formation of a PhoB heterodimer. It is not presently known whether other response regulators form heterodimers and, if so, whether heterodimer formation leads to enhanced phosphorylation kinetics. However, there is at least one published observation consistent with heterodimer formation by another response regulator. An apparent heterodimer of ComE was trapped by cross-linking and separated from the cross-linked homodimer by SDS-PAGE (51).

How the network properties of different two-component systems can result in different output behaviors, including all-or-none *versus* graded responses, is the focus of both theoretical and experimental studies (52, 53). Response regulators that form heterodimers with enhanced phosphorylation kinetics may contribute to an all-or-none output response. Our data demonstrating that phosphotransfer from the sensor kinase PhoR to PhoB was enhanced by dimer 1 formation (Fig. 8) would predict a sigmoidal relationship between phosphorylated PhoR (PhoR-P) and phosphorylated PhoB (PhoB-P) (*i.e.* a sudden nonlinear output response over a small change in input). PhoB is an autoregulated response regulator, where PhoB-P regulates transcription of both *phoR* and *phoB*, leading to a positive feedback loop for *phoB* regulation (54). In combination, the positive cooperativity and auto-regulation could lead to a physiological response that acts as an on/off switch. At low concentrations of PhoR-P, there would be little PhoB-P and thus a low level of transcriptional activation within the cell. Eventually, a threshold concentration of PhoR-P will be reached, and PhoB-P will abruptly accumulate, leading to an abrupt cellular response. There is precedent for such behavior in the all-or-none response of PhoB to phosphorylation by noncognate histidine kinases (55). Because the PhoRB system regulates transcription of genes encoding proteins involved in phosphorus assimilation, the potential on/off switch may act as a way to dampen responses to minor fluctuations in the environmental concentration of phosphate.

Because formation of dimer 1 of PhoB orients the DNA-binding domains to interact with the symmetric DNA-binding sites (29), it is possible that a PhoB heterodimer would have similar affinity for DNA and thus could regulate transcription *in vivo*. A recent study that characterizes the relationship between unphosphorylated and phosphorylated PhoB concentrations *in vivo* and transcriptional activity showed that, even at full transcriptional activity, the concentration of phosphorylated PhoB was less than the total concentration of PhoB (30). Although there are multiple explanations for this phenomenon, it could be due to a physiologically active heterodimer. If the heterodimer is active *in vivo*, there are many potential consequences. First, because the heterodimer only requires phosphorylation of a single monomer of PhoB, it will accumulate at lower concentrations of PhoB-P than the homodimer, leading to an increased sensitivity of response for the heterodimer. Second, some response regulators (*e.g.* OmpR (56), BvgA (57), and NtrC (58)) bind to different promoters with different affinities, which allows stepwise responses to changing environmental circumstances. High affinity promoters are populated at low response regulator concentrations, and promoters with low binding affinities are not populated until the concentration of response regulator is sufficiently high. The PhoB heterodimer and homodimer might exhibit different promoter binding affinities, which would facilitate a more complex regulatory scheme. Third, when the cellular signal is turned off, dephosphorylation of the PhoB homodimer may result in a functional heterodimer that can induce transcription for a longer timeframe than if no active heterodimer is formed.

Autophosphorylation of $PhoB_N$ Was Different Than CheY—Positive cooperativity was not the only parameter that differed between CheY and PhoB. Although CheY autophosphorylation was 15–30 times faster than $PhoB_N$ autophosphorylation,

$PhoB_N$ appeared to bind PAM slightly tighter than CheY. Based on our mathematical modeling, PAM binds to both the heterodimer and the monomer with binding constants (K_S(het), K_S(m)) of ~150 mM, whereas the PAM binding affinity for CheY is estimated to be greater than 500 mM (11, 15, 16). These differences in rate and binding constants were noteworthy due to the similarities in tertiary structure, active site geometry, and divalent metal coordination of $PhoB_N$ and CheY. There must be other characteristics that differ between $PhoB_N$ and CheY that can explain the differences in rate and binding constants. One hypothesis based on work on CheY where positions near to the site of phosphorylation were substituted is that a more positive charge at the active site leads to faster autophosphorylation kinetics (15). We looked at the electrostatic surface potential of the Mg^{2+}-bound forms of $PhoB_N$ (Protein Data Bank 2IYN (27)) and CheY (Protein Data Bank 2CHE (59)) using Adaptive Poisson-Boltzman Solver software (60). The surface of CheY is more positively charged than $PhoB_N$ due to residues with varying charges in nonconserved positions structurally adjacent to the active site. Because the small molecule phosphodonor is intrinsically negatively charged, the overall positive charge of the surface of CheY may lead to the faster rate of autophosphorylation compared with $PhoB_N$.

Acknowledgments—We thank Robert Immormino for assistance with mathematical modeling and for cloning and purification of PhoR; Kimberly Coggan for cloning of cheY; Aaron Moore for cloning of $phoB_F$ and $phoB_N$; Brian Crane, Robert Immormino, Stephani Page, and Stephanie Thomas for helpful discussions; and Marti Head and Peggy Cotter for comments on the manuscript.

REFERENCES

1. Capra, E. J., and Laub, M. T. (2012) Evolution of two-component signal transduction systems. *Annu. Rev. Microbiol.* **66,** 325–347
2. Ulrich, L. E., and Zhulin, I. B. (2010) The MiST2 database: a comprehensive genomics resource on microbial signal transduction. *Nucleic Acids Res.* **38,** D401–D407
3. Gao, R., and Stock, A. M. (2009) Biological insights from structures of two-component proteins. *Annu. Rev. Microbiol.* **63,** 133–154
4. Galperin, M. Y. (2010) Diversity of structure and function of response regulator output domains. *Curr. Opin. Microbiol.* **13,** 150–159
5. Gao, R., and Stock, A. M. (2010) Molecular strategies for phosphorylation-mediated regulation of response regulator activity. *Curr. Opin. Microbiol.* **13,** 160–167
6. Hess, J. F., Bourret, R. B., Oosawa, K., Matsumura, P., and Simon, M. I. (1988) Protein phosphorylation and bacterial chemotaxis. *Cold Spring Harbor Symp. Quant. Biol.* **53,** 41–48
7. Silversmith, R. E. (2010) Auxiliary phosphatases in two-component signal transduction. *Curr. Opin. Microbiol.* **13,** 177–183
8. Huynh, T. N., and Stewart, V. (2011) Negative control in two-component signal transduction by transmitter phosphatase activity. *Mol. Microbiol.* **82,** 275–286
9. Georgellis, D., Kwon, O., De Wulf, P., and Lin, E. C. (1998) Signal decay through a reverse phosphorelay in the Arc two-component signal transduction system. *J. Biol. Chem.* **273,** 32864–32869
10. Bourret, R. B. (2010) Receiver domain structure and function in response regulator proteins. *Curr. Opin. Microbiol.* **13,** 142–149
11. Da Re, S. S., Deville-Bonne, D., Tolstykh, T., V ron, M., and Stock, J. B. (1999) Kinetics of CheY phosphorylation by small molecule phosphodonors. *FEBS Lett.* **457,** 323–326
12. Lukat, G. S., McCleary, W. R., Stock, A. M., and Stock, J. B. (1992) Phosphorylation of bacterial response regulator proteins by low molecular weight phospho-donors. *Proc. Natl. Acad. Sci. U.S.A.* **89,** 718–722
13. Mayover, T. L., Halkides, C. J., and Stewart, R. C. (1999) Kinetic characterization of CheY phosphorylation reactions: comparison of P-CheA and small molecule phosphodonors. *Biochemistry* **38,** 2259–2271
14. Silversmith, R. E., Appleby, J. L., and Bourret, R. B. (1997) Catalytic mechanism of phosphorylation and dephosphorylation of CheY: kinetic characterization of imidazole phosphates as phosphodonors and the role of acid catalysis. *Biochemistry* **36,** 14965–14974
15. Thomas, S. A., Immormino, R. M., Bourret, R. B., and Silversmith, R. E. (2013) Nonconserved active site residues modulate CheY autophosphorylation kinetics and phosphodonor preference. *Biochemistry* **52,** 2262–2273
16. Schuster, M., Silversmith, R. E., and Bourret, R. B. (2001) Conformational coupling in the chemotaxis response regulator CheY. *Proc. Natl. Acad. Sci. U.S.A.* **98,** 6003–6008
17. Makino, K., Shinagawa, H., Amemura, M., Kimura, S., Nakata, A., and Ishihama, A. (1988) Regulation of the phosphate regulon of *Escherichia coli*. Activation of pstS transcription by PhoB protein *in vitro*. *J. Mol. Biol.* **203,** 85–95
18. Barbieri, C. M., and Stock, A. M. (2008) Universally applicable methods for monitoring response regulator aspartate phosphorylation both *in vitro* and *in vivo* using Phos-tag-based reagents. *Anal. Biochem.* **376,** 73–82
19. Hiratsu, K., Nakata, A., Shinagawa, H., and Makino, K. (1995) Autophosphorylation and activation of transcriptional activator PhoB of *Escherichia coli* by acetyl phosphate *in vitro*. *Gene* **161,** 7–10
20. McCleary, W. R. (1996) The activation of PhoB by acetyl phosphate. *Mol. Microbiol.* **20,** 1155–1163
21. McCleary, W. R., and Stock, J. B. (1994) Acetyl phosphate and the activation of two-component response regulators. *J. Biol. Chem.* **269,** 31567–31572
22. Lee, S.-Y., Cho, H. S., Pelton, J. G., Yan, D., Berry, E. A., and Wemmer, D. E. (2001) Crystal structure of activated CheY: comparison with other activated receiver domains. *J. Biol. Chem.* **276,** 16425–16431
23. Fiedler, U., and Weiss, V. (1995) A common switch in activation of the response regulators NtrC and PhoB: phosphorylation induces dimerization of the receiver modules. *EMBO J.* **14,** 3696–3705
24. Gao, R., Tao, Y., and Stock, A. M. (2008) System-level mapping of *Escherichia coli* response regulator dimerization with FRET hybrids. *Mol. Microbiol.* **69,** 1358–1372
25. Ames, S. K., Frankema, N., and Kenney, L. J. (1999) C-terminal DNA binding stimulates N-terminal phosphorylation of the outer membrane protein regulator OmpR from *Escherichia coli*. *Proc. Natl. Acad. Sci. U.S.A.* **96,** 11792–11797
26. Solá, M., Gomis-Rüth, F. X., Serrano, L., González, A., and Coll, M. (1999) Three-dimensional crystal structure of the transcription factor PhoB receiver domain. *J. Mol. Biol.* **285,** 675–687
27. Solà, M., Drew, D. L., Blanco, A. G., Gomis-Rüth, F. X., and Coll, M. (2006) The cofactor-induced pre-active conformation in PhoB. *Acta Crystallogr. D Biol. Crystallogr.* **62,** 1046–1057
28. Mack, T. R., Gao, R., and Stock, A. M. (2009) Probing the roles of the two different dimers mediated by the receiver domain of the response regulator PhoB. *J. Mol. Biol.* **389,** 349–364
29. Bachhawat, P., Swapna, G. V., Montelione, G. T., and Stock, A. M. (2005) Mechanism of activation for transcription factor PhoB suggested by different modes of dimerization in the inactive and active states. *Structure* **13,** 1353–1363
30. Gao, R., and Stock, A. M. (2013) Probing kinase and phosphatase activities of two-component systems *in vivo* with concentration-dependent phosphorylation profiling. *Proc. Natl. Acad. Sci. U.S.A.* **110,** 672–677
31. Skerker, J. M., Prasol, M. S., Perchuk, B. S., Biondi, E. G., and Laub, M. T. (2005) Two-component signal transduction pathways regulating growth and cell cycle progression in a bacterium: a system-level analysis. *PLoS Biol.* **3,** e334
32. Silversmith, R. E. (2005) High mobility of carboxyl-terminal region of bacterial chemotaxis phosphatase CheZ is diminished upon binding divalent cation or CheY-P substrate. *Biochemistry* **44,** 7768–7776
33. Bourret, R. B., Thomas, S. A., Page, S. C., Creager-Allen, R. L., Moore, A. M., and Silversmith, R. E. (2010) Measurement of response regulator

autodephosphorylation rates spanning six orders of magnitude. *Methods Enzymol.* **471,** 89–114
34. Sheridan, R. C., McCullough, J. F., and Wakefield, Z. T. (1972) in *Inorganic Syntheses* (Cotton, F. A., ed) Vol. 13, pp. 23–26, McGraw-Hill, New York
35. Zundel, C. J., Capener, D. C., and McCleary, W. R. (1998) Analysis of the conserved acidic residues in the regulatory domain of PhoB. *FEBS Lett.* **441,** 242–246
36. Martin, R. B. (1988) Ternary hydroxide complexes in neutral solutions of Al_3^+ and F. *Biochem. Biophys. Res. Commun.* **155,** 1194–1200
37. Kuzmic, P. (1996) Program DYNAFIT for the analysis of enzyme kinetic data: application to HIV proteinase. *Anal. Biochem.* **237,** 260–273
38. Janin, J., and Chothia, C. (1990) The structure of protein-protein recognition sites. *J. Biol. Chem.* **265,** 16027–16030
39. Fisher, S. L., Kim, S. K., Wanner, B. L., and Walsh, C. T. (1996) Kinetic comparison of the specificity of the vancomycin resistance VanS for two response regulators, VanR and PhoB. *Biochemistry* **35,** 4732–4740
40. Lukat, G. S., Stock, A. M., and Stock, J. B. (1990) Divalent metal ion binding to the CheY protein and its significance to phosphotransfer in bacterial chemotaxis. *Biochemistry* **29,** 5436–5442
41. da Silva, J. J., and Williams, R. J. (2001) *The Biological Chemistry of the Elements: The Inorganic Chemistry of Life*, 2nd ed., Oxford University Press, New York
42. Zapf, J. W., Hoch, J. A., and Whiteley, J. M. (1996) A phosphotransferase activity of the *Bacillus subtilis* sporulation protein Spo0F that employs phosphoramidate substrates. *Biochemistry* **35,** 2926–2933
43. Psakis, G., Mailliet, J., Lang, C., Teufel, L., Essen, L. O., and Hughes, J. (2011) Signaling kinetics of cyanobacterial phytochrome Cph1, a light regulated histidine kinase. *Biochemistry* **50,** 6178–6188
44. Gilles-Gonzalez, M. A., and Gonzalez, G. (1993) Regulation of the kinase activity of heme protein FixL from the two-component system FixL/FixJ of *Rhizobium meliloti. J. Biol. Chem.* **268,** 16293–16297
45. McCleary, W. R., and Zusman, D. R. (1990) Purification and characterization of the *Myxococcus xanthus* FrzE protein shows that it has autophosphorylation activity. *J. Bacteriol.* **172,** 6661–6668
46. Barbieri, C. M., Mack, T. R., Robinson, V. L., Miller, M. T., and Stock, A. M. (2010) Regulation of response regulator autophosphorylation through interdomain contacts. *J. Biol. Chem.* **285,** 32325–32335
47. Yan, D., Cho, H. S., Hastings, C. A., Igo, M. M., Lee, S.-Y., Pelton, J. G., Stewart, V., Wemmer, D. E., and Kustu, S. (1999) Beryllofluoride mimics phosphorylation of NtrC and other bacterial response regulators. *Proc. Natl. Acad. Sci. U.S.A.* **96,** 14789–14794
48. Weber, G. (1972) Ligand binding and internal equilibria in proteins. *Biochemistry* **11,** 864–878
49. Volkman, B. F., Lipson, D., Wemmer, D. E., and Kern, D. (2001) Two-state allosteric behavior in a single-domain signaling protein. *Science* **291,** 2429–2433
50. Dyer, C. M., and Dahlquist, F. W. (2006) Switched or not? the structure of unphosphorylated CheY bound to the N terminus of FliM. *J. Bacteriol.* **188,** 7354–7363
51. Hung, D. C., Downey, J. S., Kreth, J., Qi, F., Shi, W., Cvitkovitch, D. G., and Goodman, S. D. (2012) Oligomerization of the response regulator ComE from *Streptococcus mutans* is affected by phosphorylation. *J. Bacteriol.* **194,** 1127–1135
52. Kierzek, A. M., Zhou, L., and Wanner, B. L. (2010) Stochastic kinetic model of two component system signalling reveals all-or-none, graded and mixed mode stochastic switching responses. *Mol. Biosyst.* **6,** 531–542
53. Goulian, M. (2010) Two-component signaling circuit structure and properties. *Curr. Opin. Microbiol.* **13,** 184–189
54. Shinagawa, H., Makino, K., and Nakata, A. (1983) Regulation of the *pho* regulon in *Escherichia coli* K-12. Genetic and physiological regulation of the positive regulatory gene *phoB. J. Mol. Biol.* **168,** 477–488
55. Zhou, L., Grégori, G., Blackman, J. M., Robinson, J. P., and Wanner, B. L. (2005) Stochastic activation of the response regulator PhoB by noncognate histidine kinases. *J. Integr. Bioinform.* 2:11
56. Head, C. G., Tardy, A., and Kenney, L. J. (1998) Relative binding affinities of OmpR and OmpR-phosphate at the *ompF* and *ompC* regulatory sites. *J. Mol. Biol.* **281,** 857–870
57. Decker, K. B., James, T. D., Stibitz, S., and Hinton, D. M. (2012) The *Bordetella pertussis* model of exquisite gene control by the global transcription factor BvgA. *Microbiology* **158,** 1665–1676
58. Magasanik, B. (1996) in *Escherichia coli and Salmonella: Cellular and Molecular Biology* (Neidhardt, F. C., ed) 2nd Ed., pp 1344–1356, American Society for Microbiology, Washington, D. C.
59. Stock, A. M., Martinez-Hackert, E., Rasmussen, B. F., West, A. H., Stock, J. B., Ringe, D., and Petsko, G. A. (1993) Structure of the Mg^{2+}-bound form of CheY and mechanism of phosphoryl transfer in bacterial chemotaxis. *Biochemistry* **32,** 13375–13380
60. Baker, N. A., Sept, D., Joseph, S., Holst, M. J., and McCammon, J. A. (2001) Electrostatics of nanosystems: application to microtubules and the ribosome. *Proc. Natl. Acad. Sci. U.S.A.* **98,** 10037–10041